Targeted Nanoscale 3D Thermal Imaging of Tumor Cell Surface with Functionalized Quantum Dots

Jun Yang,*   Hanliang Du,   Zhenhao Chai,   Zheng Ling,   Ben Q. Li,   Xuesong Mei

Dr.J.Yang, H.L.Du, Z.H.Chai, Z.Ling, Prof.X.S.Mei

State Key Laboratory for Manufacturing Systems Engineering, Xi'an Jiaotong University, Xi'an, 710049, China

Shaanxi Key Laboratory of Intelligent Robots, Xi'an Jiaotong University, Xi'an, 710049, China

E-mail: softyj@xjtu.edu.cn

Prof.B.Q.Li

Department of Mechanical Engineering, College of Engineering and Computer Science, University of Michigan, MI 48128, USA

Abstract: Measuring the changes in tumor cell surface temperature can provide insights into cellular metabolism and pathological features, which is significant for targeted chemotherapy

and hyperthermic therapy. However, conventional micro-nano scale methods are invasive and can only measure the temperature of cells across a single plane, which excludes specific organelles. In this study, we functionalized fluorescence quantum dots (QDs) with the membrane transport protein transferrin (Tf) as a thermo-sensor specific for tumor cell membrane. The covalent conjugation was optimized to maintain the relative fluorescence intensity of the Tf-QDs to >90%. In addition, the Tf-QDs underwent changes in the fluorescence spectra as a function of temperature, underscoring its thermo-sensor function. Double helix point spread function (DH-PSF) imaging optical path was designed to locate the probe at nanoscale, and three-dimensional thermal imaging technology was proposed to measure the local temperature distribution and direction of heat flux on the tumor cell surface. This novel targeted nanoscale 3D thermometry method could be a highly promising tool for measuring the local and global temperature distribution across intracellular organelles.

1. Introduction

The generation and transfer of heat on the tumor cell surface are closely related to metabolic and pathological changes. Tumor tissues have typically elevated temperatures compared to normal tissues owing to their higher metabolic rates.[1] On the other hand, hyperthermia can effectively kill tumor cells by reducing their metabolic rates, enhancing the

cytotoxic effects of radiation and promoting chemotherapeutic drug release.[2] Consequently,

there is increasing interest in the tumorigenic role of thermo-responsive heat shock proteins

(HSPs),[3] and the immune responses triggered by hyperthermia-ablated tumors.[4,5]

Therefore, measuring the temperature changes and distribution in tumor tissues at the single

cell level can help monitor tumor cell metabolism, targeted drug therapy, hyperthermia

therapy etc.

Temperature changes in the micro-nano scale can be assessed by optical thermal imaging

using thermo-sensitive fluorescent probes, and quantified indirectly in terms of the

fluorescence intensity, lifetime, peak wavelength etc. Arai et al.[6] showed that Mito thermo

yellow detected temperature changes in the mitochondria, and can be used as a thermal probe

for tumor cells. Chretien et al.[7] used a fluorescent thermal probe to measure the in situ

temperature of mitochondria in human embryonic kidney cells under different physiological

conditions, and detected a 10 °C rise during respiration. Kucsko et al.[8] used the nitrogen–

vacancy centres in diamond nanocrystals to directly measure intracellular thermal changes

across a 200 nm scale. Uchiyama et al.[9] developed a cationic fluorescent nanogel

thermometer using a novel azo compound with imidazolium rings as the first cationic radical

initiator, and demonstrated cell thermal imaging with low toxicity.

Quantum dots (QDs) are nano-fluorescent particles with excellent optical properties owing

to their nanoscale size and tunable band gap, and are highly suitable probes for cellular

labeling,[10,11] *in vivo* imaging[12] and biomaterial detection.[13] Compared to fluorescent

proteins, organic dyes and other fluorescent particles, QDs have better optical stability,

higher quantum luminous efficiency and more distinct fluorescence peaks. In addition, the

temperature-dependent changes in their fluorescence spectra make them highly promising

non-contact nano-temperature probes.[14,15] Smith et al.[16] showed that QDs are stable within

the pH range of 5-7 and can withstand other environmental changes, which is very critical for

their application as temperature sensors for tumor cells. Yang et al.[17] used QDs to study the

local thermogenic changes in NIH/3T3 mouse fibroblasts, and Wei et al.[18] conjugated the

thermo-sensitive dye Rhodamine B (RhB) with biocompatible carbon dots (CDs) via a

covalent bond for measuring the temperature of living cells.

However, QDs can only measure the temperature of entire cells on a single plane rather

than that of specific organelles such as cytoplasm, nucleus, mitochondria and centrosomes in

three-dimensional space.[19] In order to assess the temperature changes across specific cellular

structures, QD probes have to be coupled with three-dimensional thermo-sensitive

imaging.[20,21] Furthermore, QDs can enter random cells via endocytosis, resulting in

prolonged retention and uncontrolled probe distribution. Therefore, QDs are functionalized

with specific proteins and other conjugates to improve their biocompatibility and

accumulation in target cells.[22] In addition, given that the permeability and transport capacity

of cell membranes are temperature-dependent, QDs functionalized with membrane-bound

transport proteins can be promising thermo-sensors for tumor cells undergoing metabolic and temperature changes.[23] Transferrin (Tf) is an iron-binding protein that interacts with the membrane-bound transferrin receptor (TfR), and transports the iron ions inside the cells.[24] Since TfR is frequently overexpressed on tumor cells, transferrin has been used for targeted delivery of anti-cancer drugs.[25,26]

In order to measure temperature changes in three-dimensional space, it is crucial to obtain the temperature readings and spatial position of the probe simultaneously. Point spread function is an effective micro nano three-dimensional positioning method,[27] and double helix point spread function (DH-PSF) can image a single point into a double helix spot containing axial information, thereby tracing the spatial positions of micro- and nanoparticles beyond the diffraction limit.[28,29] DH-PSF is widely used for three-dimensional positioning and tracing of intracellular proteins, mRNA and other biomolecules,[30-32] as well as the intracellular localization of QDs.[33]

In this study, we functionalized hydrophilic and biocompatible QDs with transferrin and positioned the probes using the DH-PSF method to synchronize spatial positioning with temperature reading, thereby achieving subcellular level three-dimensional targeted thermal imaging of tumor cells.

2. Preparation and characterization of Tf-QD thermal probes

2.1. Preparation of Tf-QDs

Mercaptosuccinic acid (MSA)-coated cadmium telluride (MSA-CdTe) QDs were synthesized by the aqueous phase method as previously described.[34]

The terminal carboxyl (-COOH) group of MSA-CdTe QDs was covalently conjugated with the amino (-NH$_2$) group of transferrin (Sigma-Aldrich) using carbodiimide hydrochloride (EDC) as the cross-linking agent[35] **(Figure 1)**. However, studies show that covalent coupling of transferrin to water-soluble QDs decreases the relative fluorescence intensity of Tf-QDs (ratio of fluorescence intensity of Tf-QDs to that of QDs) to 70%~80%.[36-38]
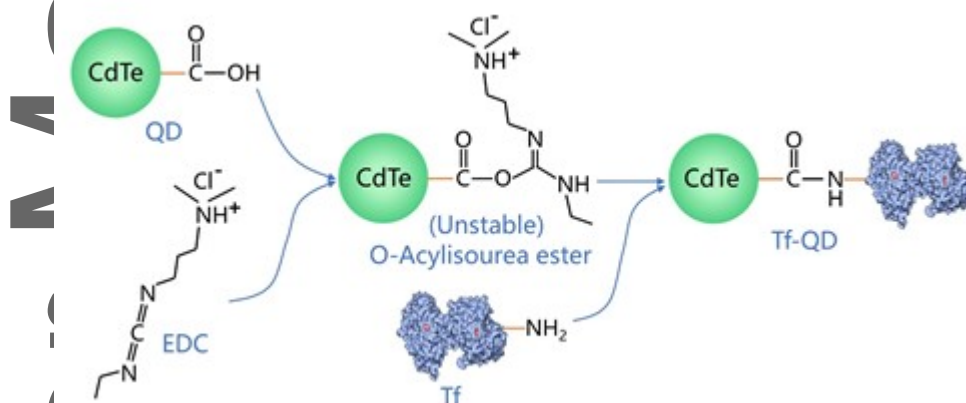

Figure 1. Principle of conjugation between quantum dots and transferrin

To optimize the fluorescence intensity of the Tf-QDs, the EDC concentration and reaction time were standardized. Briefly, 40μl QDs, 50μl Tf and 10μl EDC at different concentrations (1, 2, 5 and 10 mg ml^{-1}) were incubated for 2h, 4h and 6h respectively. As shown in **Figure 2**, the relative fluorescence intensity was > 90% with a EDC concentration of only 5 mg ml^{-1}

regardless of the reaction time. At each reaction time, the relative fluorescence intensity of Tf-QDs obtained at EDC concentration of 10 mg ml^{-1} was the lowest, which can be attributed to the corrosive effect of EDC on the thiol succinic acid coat on the QDs surface, resulting in a deep surface trap state that affects the transfer of excited electrons.[39,40] What's more, at lower EDC concentration (1 and 2 mg ml^{-1}), the reaction between QDs and Tf was insufficient, leading to the weaker relative fluorescence intensity of the obtained Tf-QDs. Therefore, 5 mg ml^{-1} EDC was selected for optimal fluorescence intensity.
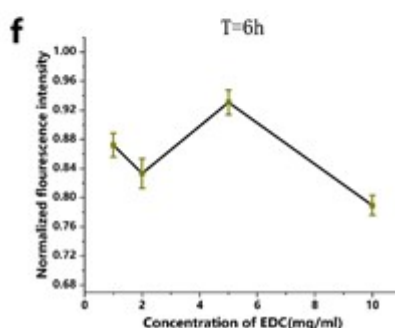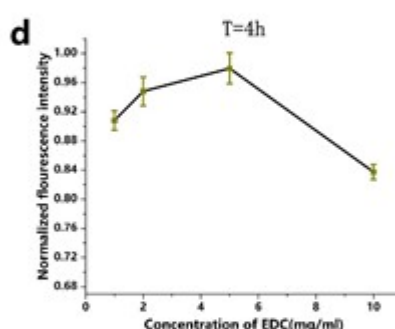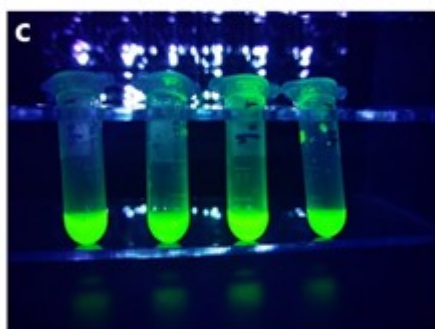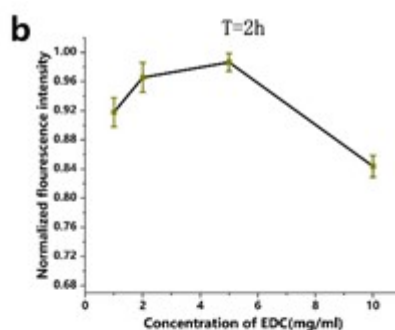
Figure 2. Effect of EDC concentration on the coupling reaction between QDs and transferrin: (a), (c), (e) Representative images showing fluorescence intensity of Tf-QDs after reaction of 2 h, 4 h and 6 h respectively (EDC concentrations from left to right were 1mg ml^{-1}, 2mg ml^{-1}, 5mg ml^{-1}, 10mg ml^{-1} respectively). (b), (d), (f) Relative fluorescence intensity of Tf-QDs at the indicated reaction times.

The 1mg ml^{-1} QDs were incubated with 5mg/ml EDC for 15 min, followed by the addition of 2 mg ml^{-1} Tf in PBS (volume ratio of EDC:QD:Tf = 1:4:5) and further incubation at 2h at room temperature under oscillation. The fully reactive solution was centrifuged at 14000g for 20 min in ultracentrifuge tubes (**Figure 3a**). The Tf-QDs captured in the nested tubes (**Figure 3b**) were resuspended in PBS and centrifuged again to remove all residues and EDC. The Tf-QDs were dispersed in PBS and stored at 4 °C for further use.
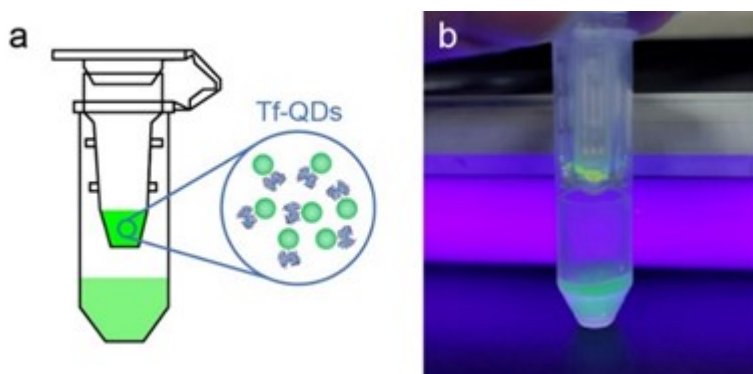

Figure 3. Centrifugal filtration of Tf-QD probes: (a) Schematic diagram of centrifugal filtration; (b) Results of centrifugal filtration.

2.2. Tumor cell targeted labeling

Human osteosarcoma cells (HOS) cells were cultured in DMEM supplemented with 10% fetal bovine serum (FBS) and 1% double anti-tumor solution at 37 °C under 5% CO_2. Once the cells were suitably confluent, functionalized or non-functionalized QD solution was added and the cells were labeled for 2 h at 37 °C. The medium was discarded and the cells

were washed twice, and then observed under an inverted fluorescence microscope. The imaging results showed that the tumor cell labeled with the Tf-QD thermal probes fluoresced intensely (**Figure 4a,b**). What's more, the fluorescence was mainly distributed on the surface of tumor cells, indicating the quantum dot probes were successfully biofunctionalized by Tf that enabled tumor cell surface targeting (**Figure 4c,d**).

2.3. Photothermal characterization of Tf-QDs

The fluorescence spectral properties of QDs are a function of temperature.[41] Although the fluorescence intensity is a measure of the number of excited probes, it decays in a time-dependent manner. In addition, the half peak width cannot be easily read from the spectral curve. The peak wavelength on the other hand is only affected by the properties of the QDs (such as material, particle size etc.) and the ambient temperature rather than the excitation parameters. Since QDs have uniform size and characteristics, the fluorescence intensity of a single probe is calculated by dividing the average intensity of the QD solution by the number of individual particles.
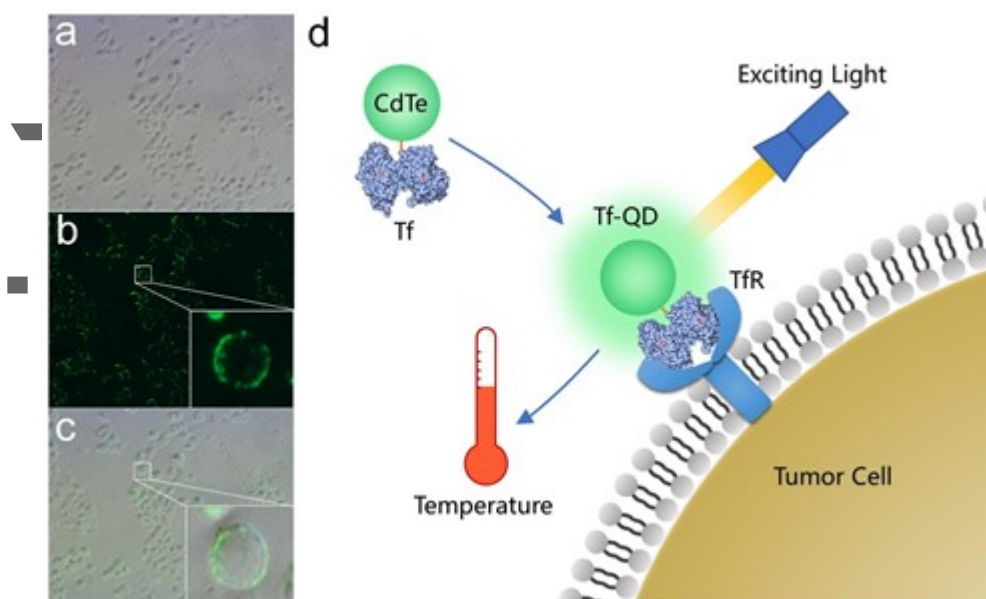
Figure 4. Representative images showing tumor cells labeled with Tf-QD targeted thermal probes: (a) Brightfield image; (b) Fluorescence image; (c) Merge image; (d) The process of Tf-QD targeted labeling to tumor cell surface.

As outlined in **Figure 5a**, the Tf-QD dispersion in PBS is placed in a water bath at room temperature and stimulated with a laser of the appropriate excitation wavelength. The emitted fluorescence is transmitted by the optical fiber to the spectrometer and the corresponding spectral curve is generated. The spectral curves are collected at different temperatures, measured in real time using a thermocouple, and the correlation between the spectral parameters of Tf-QDs and the temperature is quantified.

The peak wavelength and temperature of each spectral curve were calculated as follows:

$$\lambda = 0.15T + 547.99 \tag{1}$$

where λ is peak wavelength (nm) and T is temperature (°C).

As shown in **Figure 5(b, c)**, the Tf-QDs underwent a red shift with an increase in temperature due to decreased band gap.[42] According to the above equation, the temperature sensitivity of the Tf-QDs was 0.15 nm °C^{-1}. Taking into account the resolution of the spectrometer at 0.1 nm, the temperature resolution was 0.67 °C.

To measure the thermal stability of the Tf-QDs, the solution was repeatedly heated to 46 °C and cooled to 20 °C, and the spectral curves were recorded at the different temperatures. As shown in **Figure 5d**, the peak wavelength fluctuated at 20 °C and 46 °C but was relatively stable within the error range (deviation fluctuation ≤ 5.9%), indicating that the probe can still return to the initial state after repeated heating or cooling and ensure accurate temperature measurement.
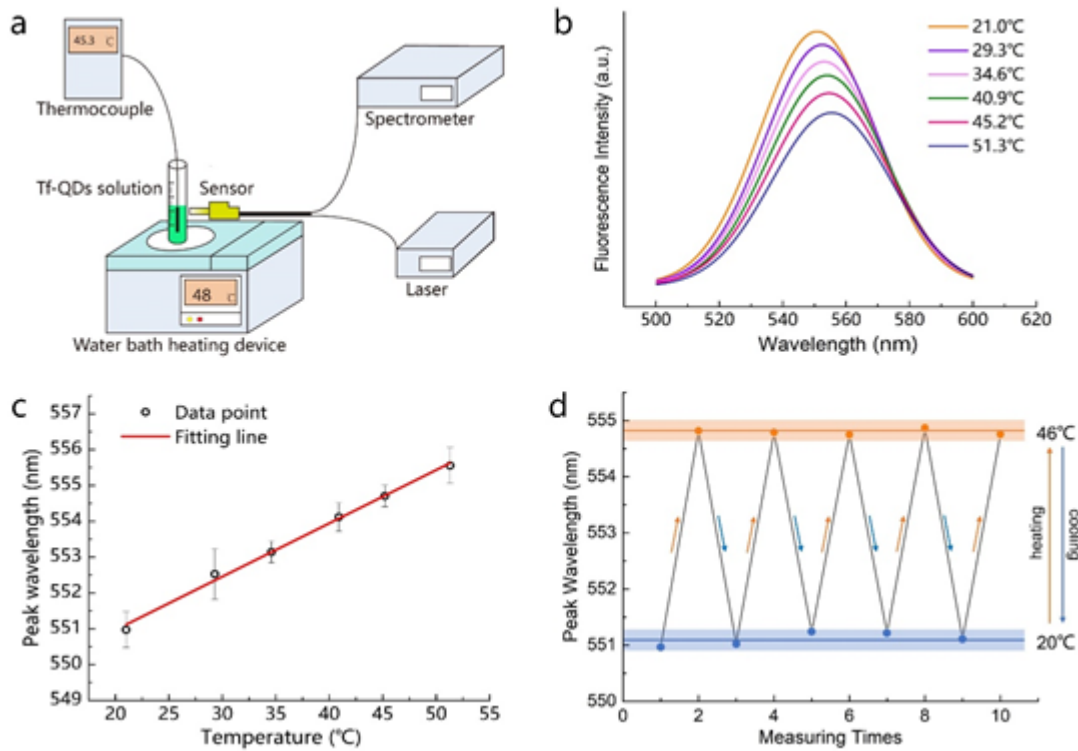
Figure 5. Variation of fluorescence spectrum of Tf-QD probes with temperature: (a) Fluorescence spectrum calibration system; (b) Fluorescence spectrum curve at different temperatures; (c) Variation of peak wavelength with temperature; (d) Thermal stability of Tf-QD probes.

3. Experiment and result analysis

3.1. Nano-scale 3D thermal imaging system

The DH-PSF is the light field distribution function obtained by imaging the point object with Laguerre-Gaussian beam, and is mathematically expressed by the paraxial approximate Helmholtz equation in cylindrical coordinate system.[43] We used a phase plate to defocus the double helix modulation of the optical path (**Figure 6a**), and the phase modulation function distribution is calculated by numerical simulation (**Figure 6b**). Fluorescent point was imaged into a specific double helix spot through this optical path. As the double spot rotated with

defocus distance (**Figure 6c**), so the Z-axis position of the target point was related to the rotation angle of the double spot quantitatively. And the XY plane position of the imaging point was located by the centroid method (see **Supporting Information** for details) to finally obtain the three-dimensional coordinate data of the probe.
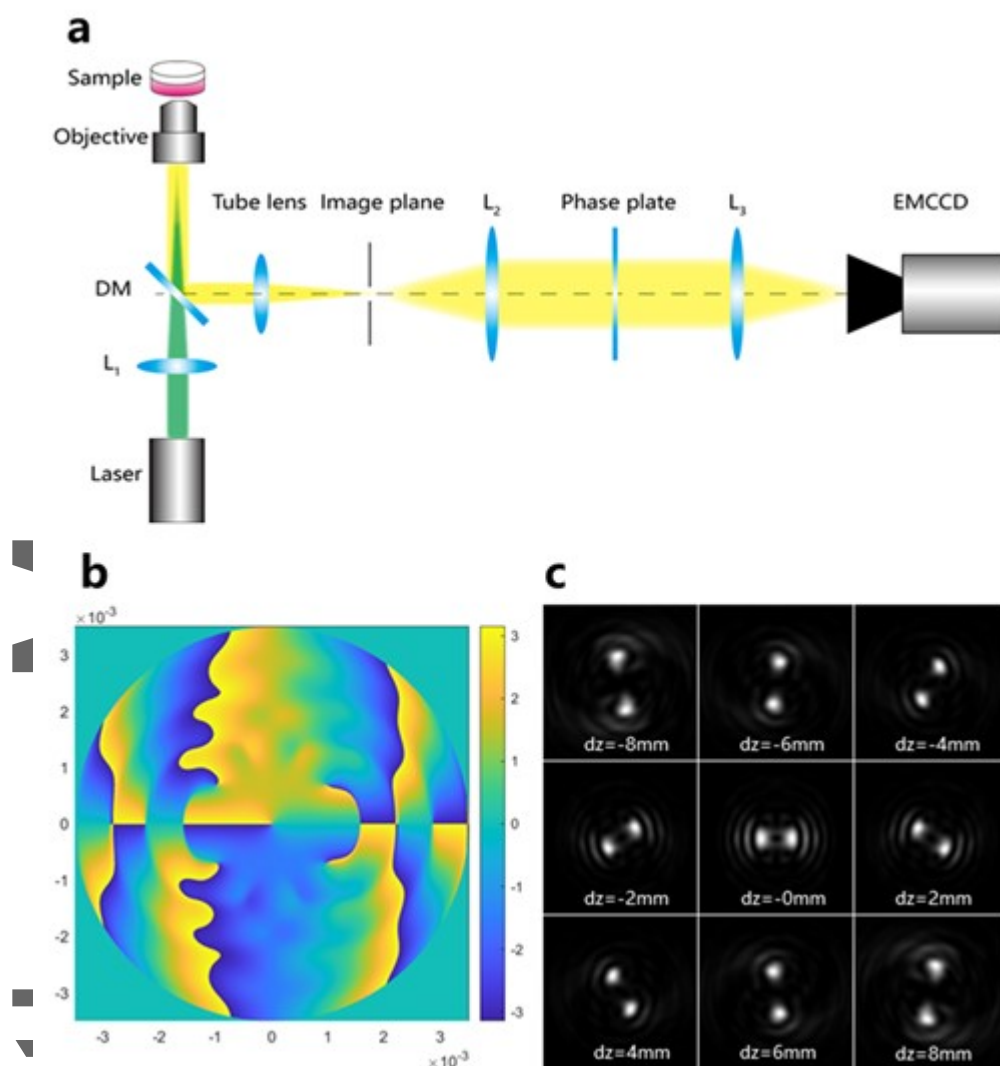

Figure 6. Defocused double helix point spread function imaging schematic: (a) Optical path of DH-PSF imaging; (b) Phase modulation function of DH-PSF imaging; (c) Variation of double spot with defocus distance.

The three-dimensional nanoscale tumor cell thermal imaging system is shown in **Figure 7**, and has been divided into three parts based on their functions: 1) fluorescence excitation and intracellular imaging of the QDs, 2) measurement of the fluorescence spectra of the probes in the field of vision, and 3) modulation of the probe spot into a double helix spot to obtain the spatial position of the probe. The system organically couples these three functions for simultaneous temperature measurement and high-precision spatial positioning of the QD probe.
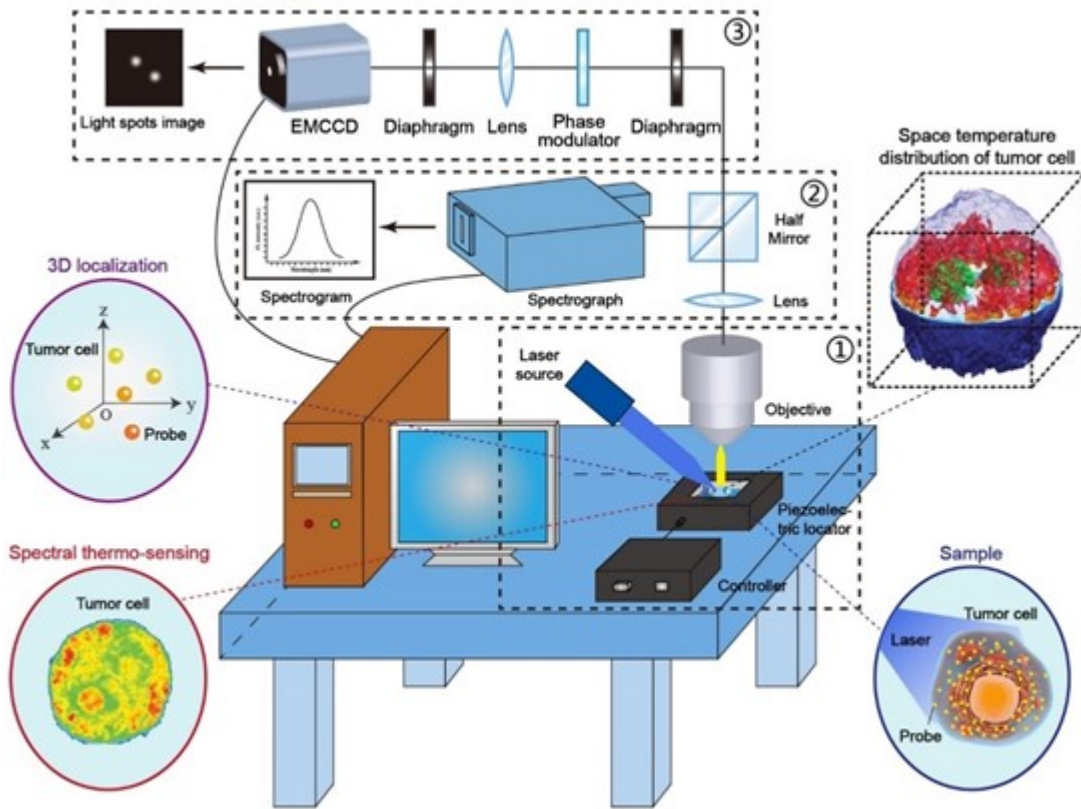

Figure 7. Tumor cell nano-scale three-dimensional thermal imaging system

The relationship between the actual axial position of the imaging point and the rotation angle of the defocusing double helix spot (**Figure 8**) is calculated as follows:

$$\theta = -0.6026\Delta z \tag{2}$$

where θ is the rotation angle of the defocusing double helix spot (rad) and Δz is the axial coordinate of the imaging point (μm).

The Z-axis axial positioning range of the system for a single imaging was about 2.6 μm (-1.5 μm ~ +1.1 μm), and since the size of the camera's photosensitive element limits the single imaging field of view to 133 μm×133 μm, the three-dimensional positioning range of a single imaging of the system is 133 μm×133 μm×2.6 μm. In addition, the calibration results showed that the lateral positioning resolution ratio of the system in the XY plane was 128 nm, and the axial positioning resolution ratio of Z- axis was 138 nm.
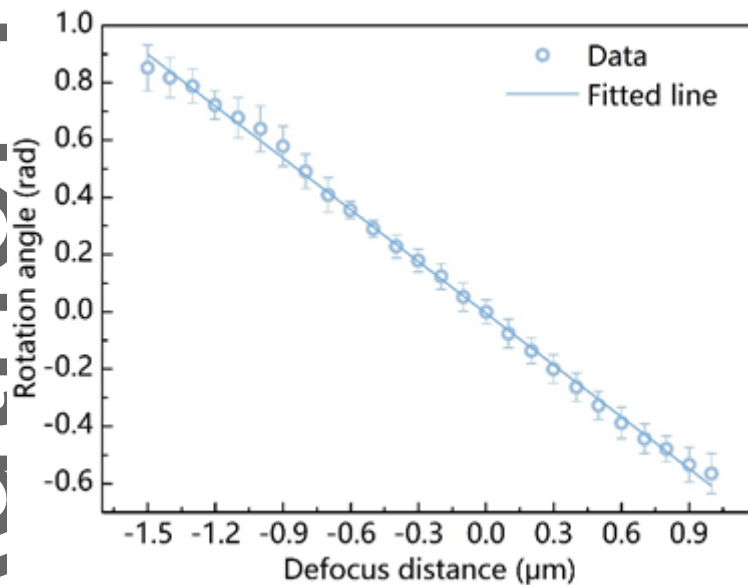

Figure 8. Relationship between axial defocusing distance and rotation angle of double light spot

3.2. Three-dimensional targeted thermal imaging of tumor cell surface

As shown in **Figure 9**, the Tf-QD probes were localized on the tumor cell surface which emitted strong fluorescence. The spectral data of five probes in the field of view (**Figure 9c**, yellow boxes) were acquired to analyze the spatial position and temperature data of the probe.

The spectral points of the selected probes were fitted using Gauss formula, and the fluorescence emission curve of each probe was obtained (solid lines, **Figure 10a**). The temperature corresponding to each peak wavelength was calculated using formula (1) (**Table 1**).

In addition, the corresponding spot center of each probe was extracted from its defocused double helix image in the dark field (**Figure 9d**) to obtain the XY plane coordinates. The angle between the center line of the double helix spot and the horizontal line corresponding to each probe was calculated, and the Z axis coordinates of the corresponding probe was obtained by formula (2) (**Table 1**). The center of the defocused double helix image was used as the origin to establish the spatial reference coordinate system (**Figure 10b**).
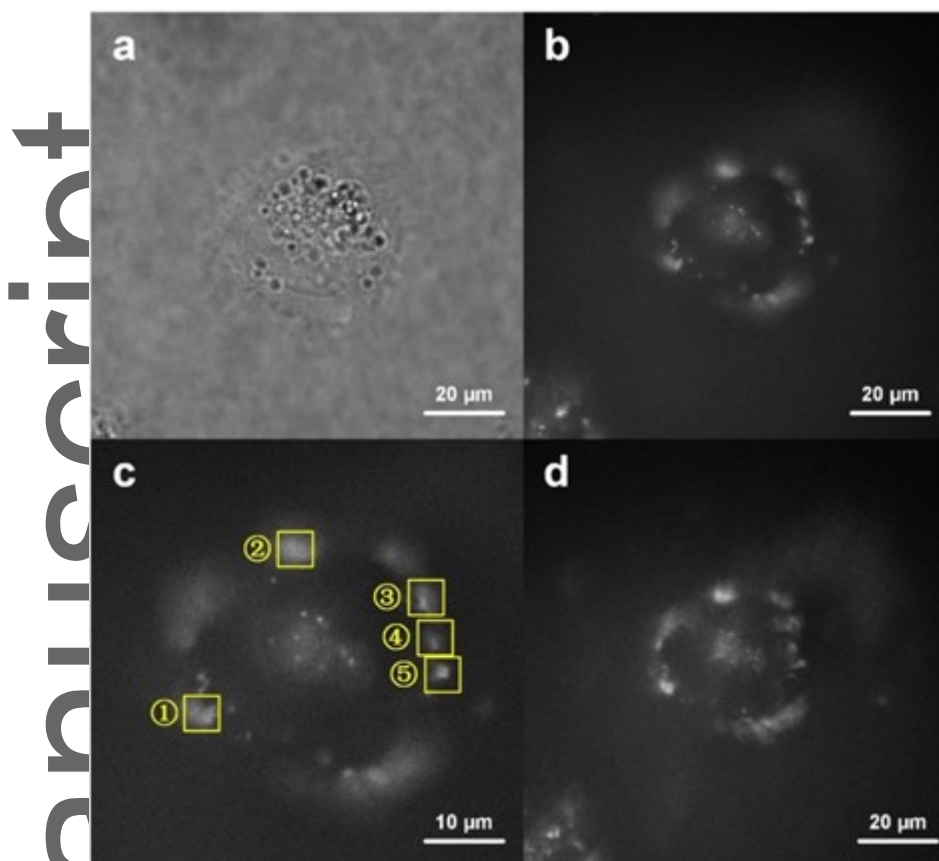
Figure 9. Results of tumor cell imaging experiment: (a) Bright field image; (b) Fluorescence image; (c) Target probe for spectral measurement; (d) Defocus double helix imaging.

Table 1. Three-dimensional coordinates and temperature values of functionalized QD probes

Probes	Double spot rotation angle /rad	Peak wavelength/nm	Spatial coordinates/μm	Temperature/°C
①	-0.661	553.030	(-18.814, 9.485, 1.098)	33.60
②	-0.166	553.216	(-3.614, -14.710, 0.276)	34.84
③	0.887	552.881	(14.491, -7.461, -1.472)	32.61
④	0.685	552.720	(14.422, -0.768 -1.137)	31.53
⑤	0.365	552.858	(16.219, 3.512, -0.606)	32.45

Based on the temperature values and three-dimensional probe coordinates, the temperature

distribution across the surface of a single tumor cell was obtained (**Figure 10c**). The average

temperature of the tumor cell surface was calculated to be 33.01 °C. As shown in **Figure 10c**, three probes (numbered 3, 4 and 5) were obliquely distributed, and the temperatures of the flanking probes were slightly higher than that of the central probe. Therefore, we surmised that the heat flux moved from the positions corresponding to probes 3 and 5 to that of probe 4. This can be attributed to the fluidity of the cell membrane, which exchanges matter and energy inside and outside all the time through phospholipid bilayers and surface receptors, and the physiological activities of adjacent regions are not identical though they influence each other. Therefore, even adjacent regions of the cell membrane have different temperature values. This provides support for the microscopic inhomogeneity of the temperature field on the surface of tumor cells. And it is of great significance for us to further explore the energy transfer pathway on the cell surface and the energy changes in the process of material transfer.
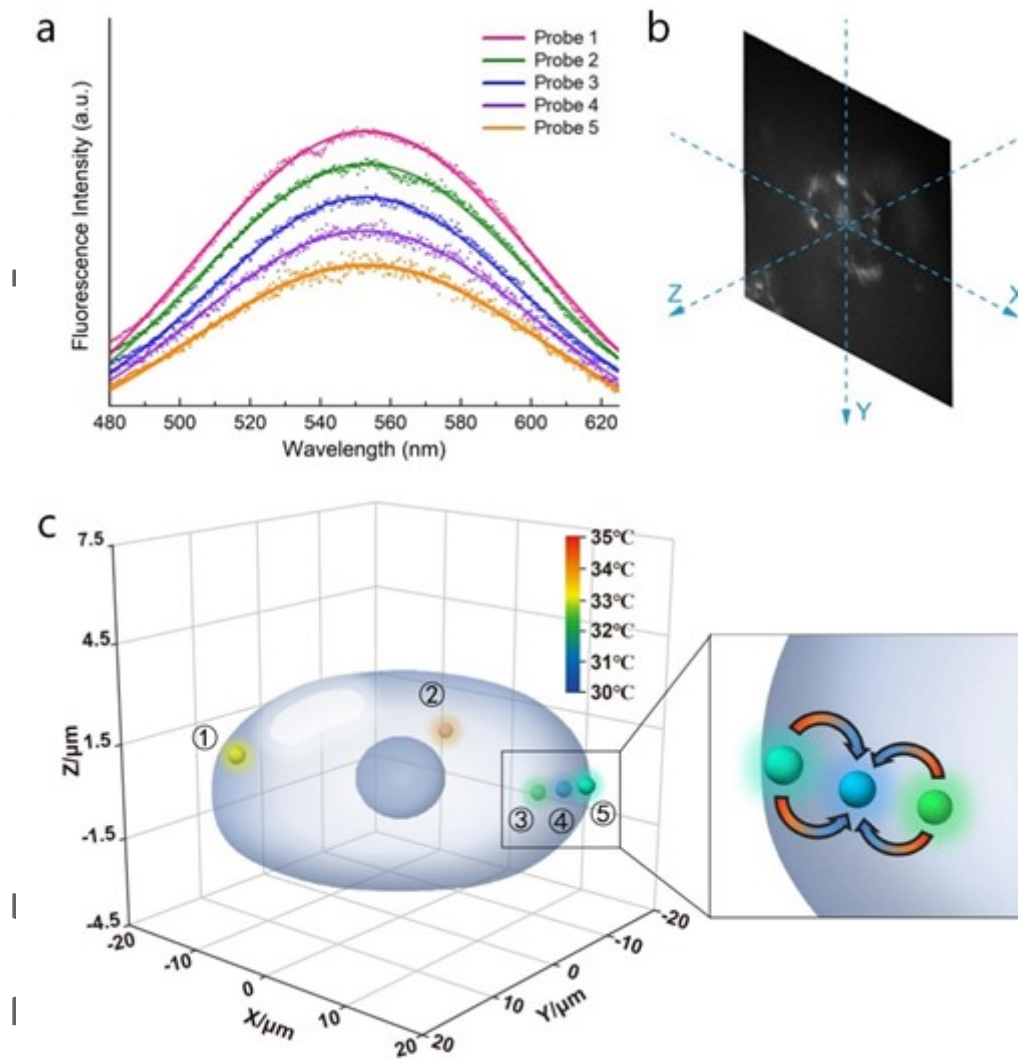
Figure 10. Three-dimensional targeted thermal imaging of tumor cell: (a) Spectral data of tumor cell surface probe and its Gaussian fitting curve; (b) Spatial reference coordinate system for image analysis; (c) Local spatial temperature distribution on the surface of tumor cells (inset shows local heat flow direction).

4. Conclusion

A targeted 3D temperature measurement method for tumor cell surface was designed and proposed. Transferrin-functionalized fluorescent QDs were studied to measure temperature changes in tumor cell surface in three-dimensional space through the DH-PSF nanoscale

imaging method. This novel targeted 3D thermometry method could be a highly promising tool for studying the metabolic and thermogenic changes during tumorigenesis at the organelle level.

References

[1] Pitt, M. A., *Inflammopharmacology* **2015,** *23*, 17.

[2] Li, W.-S.; Wang, X.-J.; Zhang, S.; Hu, J.-B.; Du, Y.-L.; Kang, X.-Q.; Xu, X.-L.; Ying, X.-Y.; You, J.; Du, Y.-Z., *Biomaterials* **2017,** *131*, 36.

[3] Ikwegbue, P. C.; Masamba, P.; Oyinloye, B. E.; Kappo, A. P., *Pharmaceuticals* **2018,** *11*, 2.

[4] Repasky, E. A.; Evans, S. S.; Dewhirst, M. W., *Cancer Immunology Research* **2013,** *1*, 210.

[5] Chang, M.; Hou, Z.; Wang, M.; Li, C.; Lin, J., *Adv. Mater.* **2020,** *33*, 2004788.

[6] Arai, S.; Suzuki, M.; Park, S.-J.; Yoo, J. S.; Wang, L.; Kang, N.-Y.; Ha, H.-H.; Chang, Y.-T., *Chem. Commun.* **2015,** *51*, 8044.

[7] Chretien, D.; Benit, P.; Ha, H.-H.; Keipert, S.; El-Khoury, R.; Chang, Y.-T.; Jastroch, M.; Jacobs, H. T.; Rustin, P.; Rak, M., *PLoS Biol.* **2018,** *16*, e2003992.

[8] Kucsko, G.; Maurer, P. C.; Yao, N. Y.; Kubo, M.; Noh, H. J.; Lo, P. K.; Park, H.; Lukin, M. D., *Nature* **2013,** *500*, 54.

[9] Uchiyama, S.; Tsuji, T.; Kawamoto, K.; Okano, K.; Fukatsu, E.; Noro, T.; Ikado, K.; Yamada, S.; Shibata, Y.; Hayashi, T.; Inada, N.; Kato, M.; Koizumi, H.; Tokuyama, H., *Angewandte Chemie-International Edition* **2018,** *57*, 5413.

[10] Betzig, E.; Patterson, G. H.; Sougrat, R.; Lindwasser, O. W.; Olenych, S.; Bonifacino, J. S.; Davidson, M. W.; Lippincott-Schwartz, J.; Hess, H. F., *Science* **2006,** *313*, 1642.

[11] Ma, Y.; Wang, M.; Li, W.; Zhang, Z.; Zhang, X.; Tan, T.; Zhang, X.-E.; Cui, Z., *Nature Communications* **2017,** *8*, 15318.

[12] Wegner, K. D.; Hildebrandt, N., *Chem. Soc. Rev.* **2015,** *44*, 4792.

[13] Tang, C.; Zhou, J.; Qian, Z.; Ma, Y.; Huang, Y.; Feng, H., *Journal of Materials Chemistry B* **2017,** *5*, 1971.

[14] Brites, C. D. S.; Lima, P. P.; Silva, N. J. O.; Millan, A.; Amaral, V. S.; Palacio, F.; Carlos, L. D., *Nanoscale* **2012,** *4*, 4799.

[15] Zhao, H.; Vomiero, A.; Rosei, F., *Small* **2020,** *16*, 2000804.

[16] Smith, A. M.; Duan, H.; Mohs, A. M.; Nie, S., *Adv. Drug Del. Rev.* **2008,** *60*, 1226.

[17] Yang, J.-M.; Yang, H.; Lin, L., *Acs Nano* **2011,** *5*, 5067.

[18] Wei, L.; Ma, Y.; Shi, X.; Wang, Y.; Su, X.; Yu, C.; Xiang, S.; Xiao, L.; Chen, B., *Journal of Materials Chemistry B* **2017,** *5*, 3383.

[19] Okabe, K.; Inada, N.; Gota, C.; Harada, Y.; Funatsu, T.; Uchiyama, S., *Nature Communications* **2012,** *3*, 705.

[20] Yang, J.; Li, B. Q.; Li, R.; Mei, X., *Nanoscale* **2019,** *11*, 2249.

[21] Yang, J.; Ling, Z.; Li, B. Q.; Li, R.; Mei, X., *Opt. Express* **2019,** *27*, 6770.

[22] Sperling, R. A.; Parak, W. J., *Philosophical Transactions of the Royal Society a-Mathematical Physical and Engineering Sciences* **2010,** *368*, 1333.

[23] Fang, C.; Ji, F.; Shu, Z.; Gao, D., *Lab on a Chip* **2017,** *17*, 951.

[24] Kawabata, H., *Free Radical Biol. Med.* **2019,** *133*, 46.

[25] Cabral Filho, P. E.; Cabrera, M. P.; Cardoso, A. L. C.; Santana, O. A.; Geraldes, C. F. G. C.; Santos, B. S.; Pedroso de Lima, M. C.; Pereira, G. A. L.; Fontes, A., *Biochimica Et Biophysica Acta-General Subjects* **2018,** *1862*, 2788.

[26] Choi, C. H. J.; Alabi, C. A.; Webster, P.; Davis, M. E., *Proc. Natl. Acad. Sci. U.S.A.* **2010,** *107*, 1235.

[27] von Diezmann, A.; Shechtman, Y.; Moerner, W. E., *Chem. Rev.* **2017,** *117*, 7244.

[28] Badieirostami, M.; Lew, M. D.; Thompson, M. A.; Moerner, W. E., *Appl. Phys. Lett.* **2010,** *97*, 161103.

[29] Lew, M. D.; Lee, S. F.; Ptacin, J. L.; Lee, M. K.; Twieg, R. J.; Shapiro, L.; Moerner, W. E., *Proc. Natl. Acad. Sci. U.S.A.* **2011,** *108*, E1102.

[30] Thompson, M. A.; Casolari, J. M.; Badieirostami, M.; Brown, P. O.; Moerner, W. E., *Proc. Natl. Acad. Sci. U.S.A.* **2010,** *107*, 17864.

[31] Gahlmann, A.; Ptacin, J. L.; Grover, G.; Quirin, S.; von Diezmann, A. R. S.; Lee, M. K.; Backlund, M. P.; Shapiro, L.; Piestun, R.; Moerner, W. E., *Nano Lett.* **2013,** *13*, 987.

[32] Carr, A. R.; Ponjavic, A.; Basu, S.; McColl, J.; Santos, A. M.; Davis, S.; Laue, E. D.; Klenerman, D.; Lee, S. F., *Biophys. J.* **2017,** *112*, 1444.

[33] Thompson, M. A.; Lew, M. D.; Badieirostami, M.; Moerner, W. E., *Nano Lett.* **2010,** *10*, 211.

[34] Jiang, X.; Shao, J.; Li, B. Q., *Appl. Surf. Sci.* **2017,** *394*, 554.

[35] Grabarek, Z.; Gergely, J., *Anal. Biochem.* **1990,** *185*, 131.

[36] Zhang, H.-L.; Li, Y.-Q.; Zhang, M.-Z.; Zhao, Y.-D., *Journal of Biomedical Optics* **2010,** *15*, 045003.

[37] Guan, L.-Y.; Li, Y.-Q.; Lin, S.; Zhang, M.-Z.; Chen, J.; Ma, Z.-Y.; Zhao, Y.-D., *Anal. Chim. Acta* **2012,** *741*, 86.

[38] Cabral Filho, P. E.; Cardoso, A. L. C.; Pereira, M. I. A.; Ramos, A. P. M.; Hallwass, F.; Castro, M. M. C. A.; Geraldes, C. F. G. C.; Santos, B. S.; Pedroso de Lima, M. C.; Pereira, G. A. L.; Fontes, A., *Biochimica Et Biophysica Acta-General Subjects* **2016,** *1860*, 28.

[39] Sun, L.; Bao, L.; Hyun, B.-R.; Bartnik, A. C.; Zhong, Y.-W.; Reed, J. C.; Pang, D.-W.; Abruna, H. D.; Malliaras, G. G.; Wise, F. W., *Nano Lett.* **2009,** *9*, 789.

[40] Hines, D. A.; Kamat, P. V., *Journal of Physical Chemistry C* **2013,** *117*, 14418.

[41] Laha, S. S.; Naik, A. R.; Kuhn, E. R.; Alvarez, M.; Sujkowski, A.; Wessells, R. J.; Jena, B. P., *Nano Lett.* **2017,** *17*, 1262.

[42] Jiang, X.; Li, B. Q.; Qu, X.; Yang, H.; Liu, H., *Journal of Materials Chemistry B* **2017,** *5*, 8983.

[43] Yang, J.; Ling, Z.; Li, R.; Mei, X., *Journal of Physics D-Applied Physics* **2019,** *52*, 365401.

Measuring the temperature changes in tumor cell surface is significant for targeted chemotherapy and hyperthermic therapy. In this study, a targeted nanoscale 3D thermometry novel method was presented, which was based on transferrin functionalized fluorescence

quantum dots (Tf-QDs) as a thermo-sensor and double helix point spread function (DH-PSF)

imaging optical path to locate the probes.